Journal of Alloys and Compounds 504 (2010) 351–356

Contents lists available at ScienceDirect

Journal of Alloys and Compounds

journal homepage: www.elsevier.com/locate/jallcom

Electrical and optical properties of In_2O_3:Mo thin films prepared at various Mo-doping levels

S. Kaleemulla[a,*], N. Madhusudhana Rao[a], M. Girish Joshi[a], A. Sivasankar Reddy[c], S. Uthanna[b], P. Sreedhara Reddy[b]

[a] Thin Films Laboratory, Department of Physics, VIT University, Vellore 632014, India
[b] Department of Physics, Sri Venkateswara University, Tirupathi 517502, India
[c] Department of Mechanical Engineering, University of Coimbra, Coimbra, Portugal

ARTICLE INFO

Article history:
Received 18 November 2009
Received in revised form 17 May 2010
Accepted 21 May 2010
Available online 27 May 2010

PACS:
68.55.Jk
73.61.−r
78.55.−m

Keywords:
Indium oxide
Activated reactive evaporation
Transparent conducting oxide

ABSTRACT

The optically transparent conducting molybdenum-doped indium oxide thin films (In_2O_3:Mo) were prepared on glass substrates by an activated reactive evaporation method and the influence of molybdenum doping levels on the electrical and optical properties of the films had been investigated systematically. The films, synthesized at a substrate temperature of 573 K and a Mo-doping level of 3 at.%, exhibited a minimum electrical resistivity of $5.2 \times 10^{-4}\ \Omega$ cm and an average optical transmittance of 90% in the visible region with a band gap of 3.68 eV.

1. Introduction

In the present era, the science of thin films and its relative technologies are playing an important role in our daily life as they are found in number of applications from microelectronics to automobile parts. These applications are highly depending on the physical properties of the materials that have been chosen. The properties of thin films were highly influenced by structure, morphology, stoichiometry of the films and nature of the impurity added. To meet the current need of the optoelectronic applications such as flat panel displays, photovoltaic cells, smart windows, light emitting diodes and optical wave guides, solar cell, touch panel controls, electromagnetic shielding of CRT used for video display terminals, the thin films should have high electrical conductivity and maximum optical transmittance in the visible region [1,2]. Hence transparent conducting oxides (TCOs) became the essential part of the above said applications.

TCOs are the materials which exhibit unique properties such as low electrical resistivity ($<10^{-3}\ \Omega$ cm), high optical transmittance in the visible region (>80%) and high infrared reflectance with a wide band gap [3,4]. The efficiency and performance of the optoelectronic devices depend on the electrical and optical properties of the TCO materials used in their construction. As the optical transmittance and electrical resistivity are controversial to each other, a careful balance between the optical and electrical properties is required to achieve the highest optical transmittance at the highest electrical conductivity. The electrical conductivity of the TCO films can be increased by increasing either carrier concentration or mobility of the carriers. The carrier concentration of the oxide materials can be increased either by adding external impurities or making the films off-stoichiometric in nature. The carriers are generated due to the valence difference between doped ions and substituted ions in the matrix oxides. Then the excess electrons will appear in the conduction band. These electrons are loosely bonded with the doped ions. Hence a lesser amount of energy is enough for them to become free carriers [5]. Oxygen vacancy is another way to offer free carriers. Each oxygen vacancy can donate two electrons to the conduction band. Hence an increase in oxygen vacancy can increase the free carrier concentration [6,7]. But at the same time carrier concentration has a diverse influence on the optical property of the TCO films due to the plasma resonance [8].

Since the mobility is directly proportional to relaxation time and inversely proportional to the effective mass of the carriers, the

* Corresponding author. Tel.: +91 900 33 86732.
E-mail address: skaleemulla@gmail.com (S. Kaleemulla).

0925-8388/$ – see front matter © 2010 Elsevier B.V. All rights reserved.
doi:10.1016/j.jallcom.2010.05.068

Table 1
Deposition parameters of the IMO films during the preparation.

Source material	(99.999%) in metal specs, MoO_3 powder
Substrates	Corning 7059 glass slides (75 mm × 25 mm × 1 mm)
Source to substrate distance	120 mm
Base pressure in the chamber	3×10^{-6} mbar
Oxygen partial pressure (PO_2)	2×10^{-3} mbar
Substrate temperature (T_s)	573 K
Mo-doping levels	0–5 at.%

mobility of the charge carriers can be enhanced either by increasing relaxation time due to fewer defects or by reducing the effective mass of the carriers. Hence a suitable material with appropriate parameters is necessary to achieve the good electrical conductivity with moderate optical transmittance.

Among the various available TCOs like, CdO, ZnO, SnO_2, the In_2O_3 is the best TCO as it can be tailored as a conductor or semiconductor or even insulator. If impurities are added to In^{+3}, electrons will be added to the empty 5s and 5p levels. The impurities like tin (Sn), gallium (Ga), copper (Cu), zirconium (Zr), erbium (Er) and titanium (Ti) have been doped into the In_2O_3 matrix and studied extensively by many researchers [9–14]. Compared to these dopants, Mo ([Kr]: $4d^5 5s^1$) is the more beneficial impurity to be doped into the In_2O_3 matrix as it can donate more than three electrons to the free carriers due to the high valence difference between Mo^{+6} ions and substituted In^{+3} ions. A variety of deposition techniques such as thermal evaporation, electrodeposition, radio frequency magnetron sputtering and high density plasma evaporation [15–18] have been employed for the preparation of undoped and molybdenum-doped indium oxide thin films (IMO).

In the present work, Mo-doped indium oxide thin films were prepared by the thermally activated reactive evaporation (ARE) method which is particularly designed for the preparation of oxides and nitrides films. The influence of Mo-doping level on the structural, optical and electrical properties of the films was studied systematically.

2. Experimental procedures

2.1. IMO films preparation

In_2O_3:Mo thin films were prepared using a home built activated reactive evaporation method. The ARE technique has many advantages since the reaction occurs predominantly in the plasma by which even high melting point inorganic compounds can be synthesized at lower temperatures. Thin films of molybdenum-doped In_2O_3 (IMO) were prepared in 12 in. vacuum coating unit (Model: 12A4D) consisted of a resistively heated boat in which the source to substrate distance could be varied in the range of 120 mm. The vacuum system consists of a diffusion pump backed by a rotary pump. The pressure in the vacuum chamber was measured using Pirani and Penning gauges. After attaining the base pressure of 3×10^{-6} mbar, pure oxygen gas (99.999%) was admitted into the vacuum chamber through a fine controlled needle valve. The flow of the reactive gas was controlled by Tylon mass flow controller (MFC). Pure indium (99.999%) and MoO_3 were used as source materials for the deposition of the IMO films. A dc power supply of 1 A and 1000 V was used to produce the discharge. The IMO films were deposited on well cleaned glass substrates held at temperature of 573 K under various Mo-doping levels in the range 0–5 at.%. The deposition conditions maintained during the preparation of the IMO films were tabulated in Table 1.

2.2. IMO films characterization

The deposited IMO films were characterized for the crystallographic structure, surface, electrical and optical properties. The thickness of the films was determined from the interference of the optical transmittance. The crystallographic structure of the films was determined by employing Seifert X-ray diffractometer with the copper k_α radiation of wavelength 1.5406 Å. The surface morphology of the films was examined by scanning electron microscope (SEM) (JSM-840A) and atomic force microscope (AFM) (Veeco-CP-2). The elemental composition of the layers was studied using VG Microtech ESCA2000 X-ray photoelectron spectrometer (XPS). The optical transmittance (T%) of the films was recorded using Hitachi U-3400 UV–vis–NIR double beam spectrophotometer with a bare glass substrate in the path of the reference beam in the wavelength range 300–1000 nm. By applying electrical current using Advantest programmable dc voltage/current generator (Model: TR 6142), the voltage drop across the film was measured with (make H P) multimeter. The electrical resistivity of the deposited films was measured using standard van der Pauw method [19].

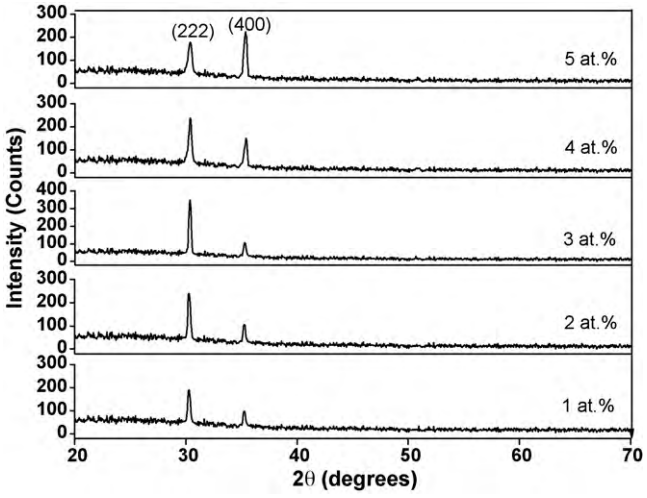

Fig. 1. X-ray diffraction patterns of the IMO films at various Mo-doping levels.

3. Results and discussion

Fig. 1 shows the X-ray diffraction patterns (XRD) of the IMO films as a function of Mo-doping levels in 2θ range 20–70°. All the diffracted peaks as labeled were coincided with intrinsic In_2O_3 cubic structure [20]. No significant change in the crystal structure was observed with the increase in doping levels. But the change in preferential orientation of the IMO films was observed at higher Mo-doping levels.

The films were oriented along (2 2 2) and (4 0 0) planes in which (2 2 2) orientation is more predominant. The intensity of the diffracted peaks increased as the Mo-doping level increased from 1 to 3 at.%, thereafter the intensity of the films slightly decreased and the intensity of (4 0 0) orientation started to increase from 4 to 5 at.%. The strongest diffraction peak of the films changed from the (2 2 2) to plane to the (4 0 0) plane. If the dopant occupies interstitial sites of the respective ion, the change in the preferred orientation may not occur. However, if the dopant occupies additional interstitial sites which are unoccupied, a change in the preferred growth takes place. In the present study it seems that Mo replaces indium at its regular lattice sites up to 3 at.% of Mo-doping levels. At higher Mo-doping levels, perhaps the Mo incorporated at additional interstitial sites which results the change in preferred orientation of the films. The change in preferential orientation was also observed in Sn-doped In_2O_3 films by Agashe and Mahamuni [21]. No significant shift in 2θ of the XRD peak was observed at lower doping levels (3 at.%.) which indicates that Mo^{+6} ions substituted In^{+3} ions in the In_2O_3 matrix without significantly affecting the lattice parameter. It may be due to smaller ionic radius of Mo^{+6} (0.62 Å) than that of In^{+3} (0.81 Å). Similar results were also observed in sputtered Ti-doped In_2O_3 thin films [22]. But the XRD peaks showed slight shift to the higher diffraction angles in Ga-doped In_2O_3 thin films [23]. A change in growth orientation from (2 2 2) to (4 0 0) peak at a Mo-doping level of 2 at.%. was observed in spray deposited IMO films [24]. The grain size of the films was estimated by the Debye–Scherrer relation $t = 0.9\lambda/\beta\cos\theta$, where λ is the wavelength of the X-rays, β is the full width at half maximum (FWHM) of (2 2 2) diffracted peak at $2\theta = 30.5°$ and θ is the diffraction angle of the XRD spectra. The grain size of the films increased from 18 to 33 nm with the increase of the Mo-doping level from 1 to 3 at.%, after which it

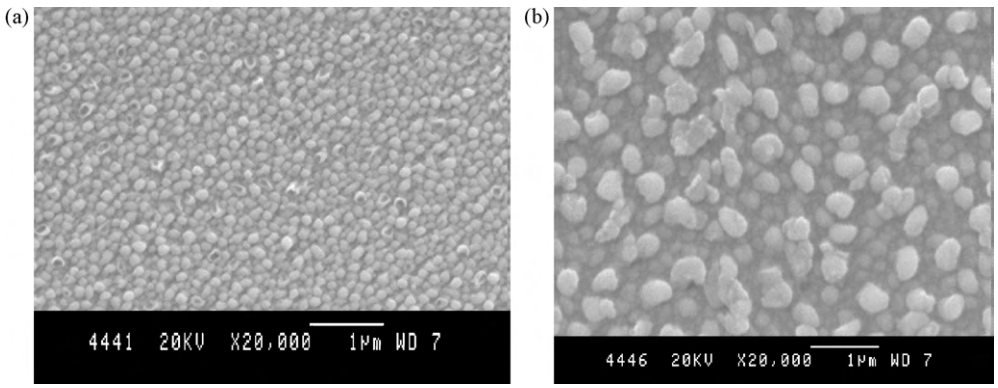

Fig. 2. SEM images of the IMO films with (a) 1 at.% and (b) 3 at.% Mo-doping level.

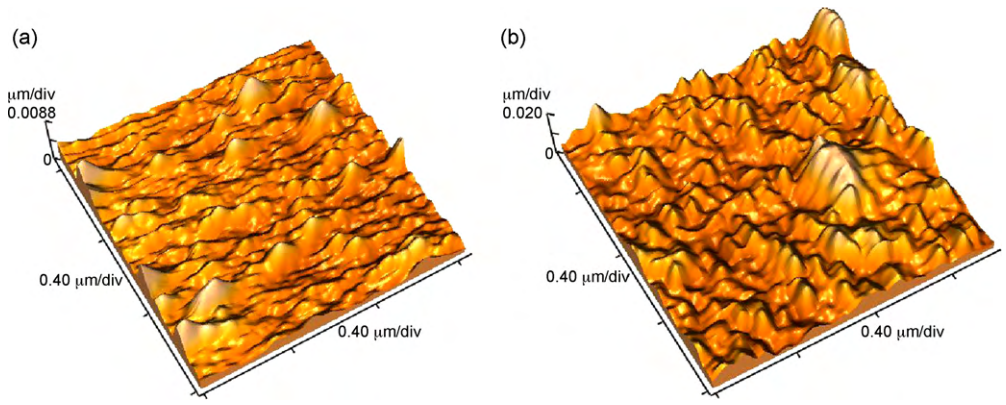

Fig. 3. The AFM images of the IMO films with (a): 3 at.% and (b) 5 at.% Mo-doping level.

remained constant (~30 nm) at higher doping levels. Similar results were also observed in spray deposited Ga-doped ZnO films [25]. But a decrease in the grain size with increase in doping concentration was observed in vanadium doped ZnO films [26].

Fig. 2(a) and (b) shows the scanning electron microscope (SEM) images of the IMO films formed and at 1 and 3 at.% of Mo-doping levels. The small, spherical grains were distributed throughout the substrate surface at lower doping level (1 at.%). As the doping level increased to 3 at.%, an increase in the grain size was observed. The grain size observed from the SEM image is closer to the mean grain size calculated by the XRD data.

Fig. 3(a) and (b) shows the three dimensional (3D) AFM images of the samples formed at lower (3 at.%) and higher Mo-doping levels (5 at.%). The AFM images were scanned for the area of 1 μm × 1 μm. The surface morphology of the TCO electrode is very important since it directly affects the surface morphology of organic materials deposited on it [27]. A smooth surface with uniform grains in pyramid shape were distributed over the substrate surface for the films deposited at a Mo-doping level of 3 at.%. The RMS roughness of the films formed at lower Mo-doping levels was ~1.1 nm, after which it increased to 1.8 nm at higher doping level (5 at.%) due to the uneven sizes of the grains, which reflects that large concentrations may affect the crystal structure.

Fig. 4(a) and (b) shows the elemental composition of the layers of In $3d_{3/2}$, In $3d_{5/2}$, Mo $3d_{3/2}$ and Mo $3d_{5/2}$ for the IMO films formed at a substrate temperature of 573 K and at a Mo-doping

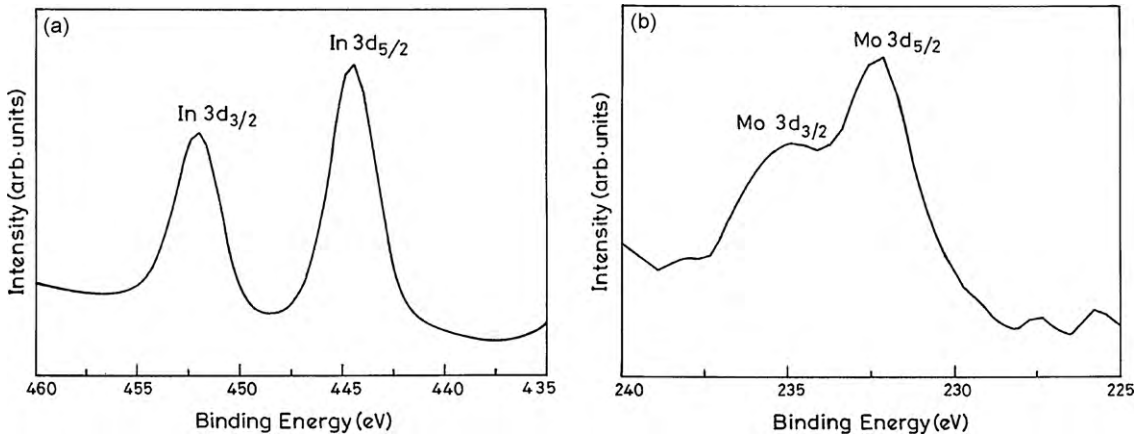

Fig. 4. (a) XPS spectra of the In 3d and (b) Mo 3d films formed at 3 at.% of Mo-doping levels.

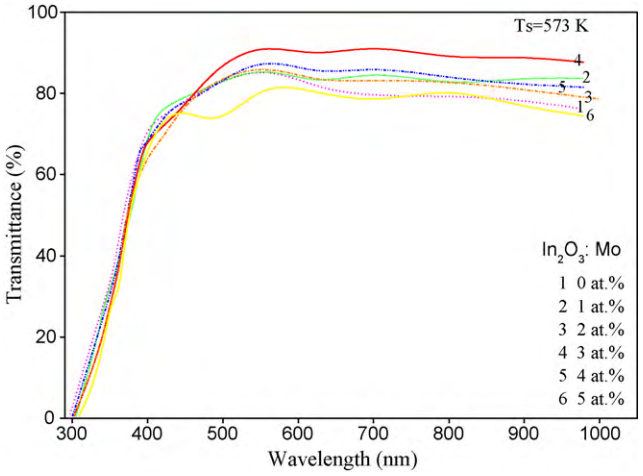

Fig. 5. Optical transmittance spectra of the IMO films at various Mo-doping levels.

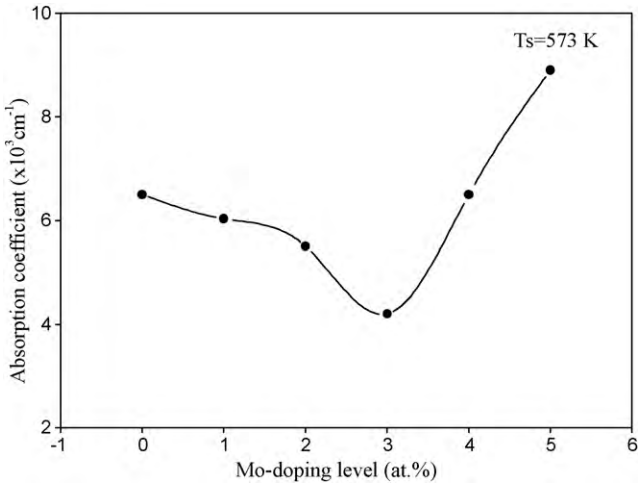

Fig. 6. Variation of the absorption coefficient of the IMO films as a function of Mo-doping level.

level of 3 at.%. The binding energies of In $3d_{5/2}$, In $3d_{3/2}$, Mo $3d_{5/2}$ and Mo $3d_{3/2}$ were found to be as 444.40, 452.3, 232.3 and 235.8 eV, respectively. The observed binding energies are close enough to the binding energies of IMO films deposited at a Mo-doping level of 4.62 at.% using spray pyrolysis technique [28] in which the binding energies of the In $3d_{5/2}$, In $3d_{3/2}$, Mo $3d_{5/2}$ and Mo $3d_{3/2}$ were found as 444.9, 452.5, 232.7 and 235.9 eV, respectively.

Fig. 5 shows the optical transmittance spectra of the IMO films as a function of Mo-doping levels in the wavelength ranging 300–1000 nm. In Fig. 5 (1–6) are the optical transmission spectra of the IMO films prepared with Mo-doping levels of 0, 1, 2, 3, 4 and 5 at.%, respectively. The undoped In_2O_3 thin films exhibited an average optical transmittance of 83% after which it increased to 90% with the increase of Mo-doping level from 1 to 3 at.%. The increase in transmittance is related to an increase in crystallanity of the films at lower Mo-doping levels (up to 3 at.%). Since the carrier concentration has a distinct influence on the optical properties of the TCO films due to plasma resonance [8], a decrease in the optical transmittance (80%) of the films was observed at higher doping levels (5 at.%). The data for the sheet resistance, the transmittance and the figure of merit is summarized in Table 2. The absorption coefficient (α) of the films was calculated using the relation:

$$T = Ae^{-\alpha t} \quad (1)$$

where A is a constant, T is the optical transmittance and 't' is the thickness of the film.

Fig. 6 shows the variation of absorption coefficient of the IMO films with Mo-doping levels. The absorption coefficient of the IMO films decreased from 6.5 to 4.2×10^3 cm^{-1} with the increase of Mo-doping level from 0 to 3 at.%. A less absorbance was observed at lower Mo-doping levels, after which it increased to 8.9×10^3 cm^{-1} at higher Mo-doping level (5 at.%).

Fig. 7 shows the optical band gap of the IMO films formed at 0, 3 and 5 at.% of Mo-doping levels. The optical band gap (E_g) for highly degenerate semiconducting oxides can be determined from the absorption coefficient (α) and photon energy ($h\upsilon$) using the

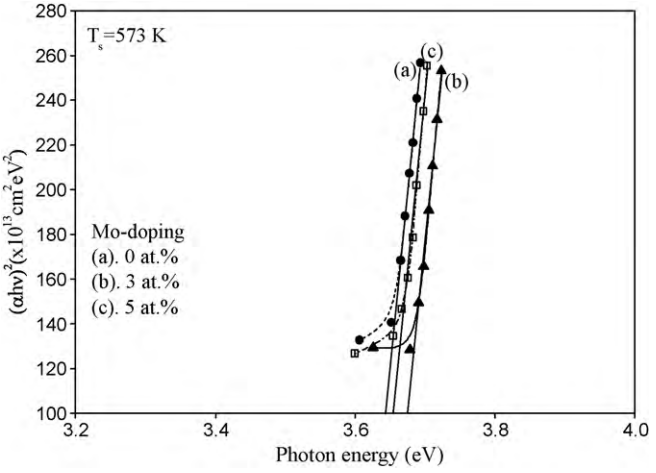

Fig. 7. Optical band gap of the IMO films formed at 0, 3 and 5 at.% of Mo-doping levels.

following relation [29]:

$$\alpha h\upsilon = A(E_g - h\upsilon)^{1/2} \quad (2)$$

The optical bang gap E_g is obtained by plotting $(\alpha h\upsilon)^2$ versus the photon energy ($h\upsilon$) and by extrapolating the linear region of the plots to zero absorption ($\alpha = 0$). At a substrate temperature of 573 K the optical band gap of the films increased from 3.64 to 3.68 eV as the Mo-doping level increased from 1 to 3 at.%. The change of the optical band gap of IMO thin films is bound up with the valence state of the Mo ions. If Mo ions occupy the lattice sites replacing In ions, they will provide additional free carriers which cause the Fermi level to move into conduction band causing an increase in the optical band gap. The observed optical band gap is close to optical band gap of the spray deposited IMO films [30]. At higher doping

Table 2
Summary of sheet resistance, transmittance and figure of merit as a function of Mo-doping levels.

Mo-doping level (%)	Sheet resistance (/□)	Transmittance (T%)	Figure of merit ($\times 10^{-3}\ \Omega^{-1}$)
0	30.5	83	5.09
1	35.2	86	6.28
2	30.0	87	8.28
3	20.8	90	16.0
4	23.2	85	8.40
5	25.2	80	4.20

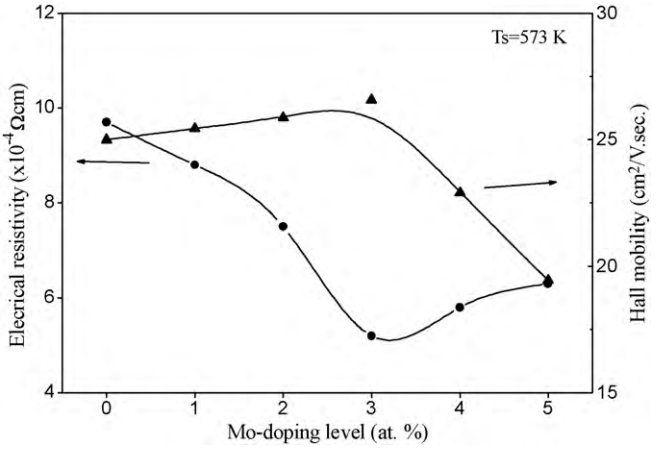

Fig. 8. Variation of the electrical resistivity and mobility of the IMO films with Mo-doping levels.

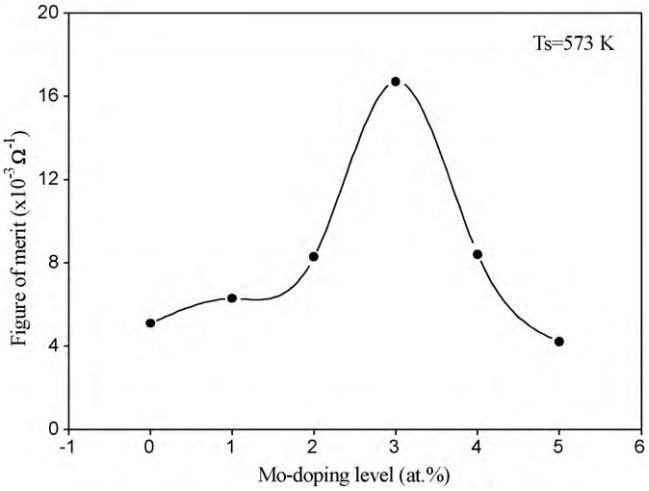

Fig. 9. Variation of the figure of merit of IMO films as a function of Mo-doping level.

levels (5 at.%) it decreased to 3.64 eV which may be due to lattice distortion. Generally a band gap of 3.5 eV is essential for the TCO in most anticipated optoelectronic applications [31] and the films in this investigation fulfilled the basic requirement.

Basically, it is known that for TCO films the conduction electrons are normally supplied by doping donars and/or oxygen vacancies. In the process of doping, the donor ions substitute the cations in parent oxides and provide extra electrons to the conduction band. This is due to the valence difference between doped ions and substituted ions. The conductive mechanism of TCO films can be explained by Kroger–Vink defect models [K–V notation] [32] of compensation mechanism and donor mechanism [33]. According to this model, the substitution of Sn dopant in ITO is compensated by interstitial oxygen so as to lose activation, thus will not contribute to the carrier concentration i.e. two Sn^{+4} substituting for In^{+3} will not contribute carriers when every neutral complex is formed. It can be written as:

$$2In_{In} + 2SnO_2 \rightarrow (2Sn_{In}^{\bullet})O_i'' + In_2O_3 \quad (3)$$

As a reminder, in K–V notation, the capital letters represent the defect or ionic species, the subscript stands for the site, and the superscript denotes the effective charge, whether negative (′) or positive (•).

But in the case of IMO, Mo^{+6} substituting for In^{+3} will contribute one carrier even after it associates with one interstitial O^{2-} without changing the cubic bixbyite structure of In_2O_3. It can be represented as:

$$2In_{In} + 2MoO_3 \rightarrow 2Mo_{In}^{\bullet\bullet\bullet}O_i'' + In_2O_3 + \frac{1}{2}O_2 + 2e' \quad (4)$$

In the model of donor mechanism, for the same dopant content, IMO film may provide much more carriers, which can be seen apparently by:

$$2In_{In} + 2MoO_3 \rightarrow 2Mo_{In}^{\bullet\bullet\bullet} + In_2O_3 + \frac{3}{2}O_2(g) + 6e' \quad (5)$$

In other words, for the same number of carrier concentration, there exist much less of dopant scattering centers in IMO films than that of in ITO films. It implies that the high valence difference between the dopant and substituted ions proved the great advantage to TCO films with good optical and electrical properties.

Fig. 8 shows the variation of electrical resistivity and mobility of the IMO films deposited at various Mo-doping levels. The undoped In_2O_3 films exhibited an electrical resistivity of $9.4 \times 10^{-4}\,\Omega\,cm$ after which it decreased to a value of $5.2 \times 10^{-4}\,\Omega\,cm$ when Mo-doping level increased to 3 at.%. The reason for the decrease in electrical resistivity is that each molybdenum impurity can donate three electrons as explained above. Hence the electrical resistivity of the IMO films decreased with the increase of doping level (3 at.%). But at higher doping levels (5 at.%), the magnitude of electrical resistivity increased up to $6.3 \times 10^{-4}\,\Omega\,cm$. It may be due to the increase of impurity scattering which decreases the mobility of the charge carriers. Similar increase of resistivity with dopant concentration was observed in Zr-doped In_2O_3 films (IZO) [13]. The electrical resistivity observed in this investigation is lower than that of the electrical resistivity of the ion beam assisted Mo-doped In_2O_3 thin films [34].

An increase in Hall mobility was observed for the films deposited in the dopant concentration from 0 to 3 at.%. The films exhibited a higher mobility of 26.58 $cm^2/V\,s$ at 3 at.% of Mo-doping level. Then it decreased to 19.45 $cm^2/V\,s$ at higher doping level (5 at.%). The films exhibited lower carrier concentration of $2.5 \times 10^{20}\,cm^{-3}$ at 0 at. % of Mo-doping level, then it increased to $5.1 \times 10^{20}\,cm^{-3}$ when the Mo-doping level increased from 1 to 5 at.%. The higher Mo-doping levels can increase the resistivity by decreasing the mobility due to impurity scattering.

Fig. 9 shows the variation of figure of merit (Φ_{TC}) with Mo-doping levels. Figure of merit is the parameter which can judge the performance of the TCO film.

Figure of merit of the films was determined using the relation [35]:

$$\Phi_{TC} = \frac{T^{10}}{\rho_s} \quad (6)$$

where T is the optical transmittance at 550 nm and ρ_s is the sheet resistance of the film.

Here the figure of merit of the IMO films increased from 5.09 to $16 \times 10^{-3}\,\Omega^{-1}$ with the increase of Mo-doping from 0 to 3 at.%. The increase in figure of merit with Mo-doping was due to the decrease in the electrical resistivity as well as increase in optical transmittance. The higher the figure of merit, the better is the performance of the transparent conducting film. The best performance of the samples was obtained at a Mo-doping of 3 at. % with $\Phi_{TC} = 16 \times 10^{-3}\,\Omega^{-1}$. The observed figure of merit investigated is better than magnetron sputtered Mo-doped In_2O_3 films [36].

4. Conclusions

Mo-doped In_2O_3 (IMO) thin films with high optical transmittance and low resistivity have been prepared using the ARE method. It was observed that the role of Mo-doping level is crucial with high impact on electrical and optical properties. The XRD studies

revealed that the films were cubic in structure and found to be predominantly oriented along (2 2 2) plane. The films deposited at Mo-doping level of 3 at.%, exhibited a highest optical transmittance of 90% in the visible region and the lowest electrical resistivity of $5.2 \times 10^{-4}\ \Omega$ cm with a figure of merit $16 \times 10^{-3}\ \Omega^{-1}$. These properties are highly suitable for most of the optoelectronic applications.

References

[1] B.S. Chua, S. Xu, Y.P. Ren, Q.J. Cheng, K. Ostrikov, J. Alloys Compd. 485 (2009) 379.
[2] R.S.D. Biasi, M.L.N. Grillo, J. Alloys Compd. 485 (2009) 26.
[3] L. Kerkache, A. Layadi, A. Mosser, J. Alloys Compd. 485 (2009) 46–50.
[4] A.A. Dakhel, J. Alloys Compd. 470 (2009) 195–198.
[5] Y. Meng, X. Yang, H. Chen, J. Shen, Y. Jiang, Z. Zhang, Z. Hua, Thin Solid Films 394 (2001) 219–223.
[6] T. Minami, Thin Solid Films 516 (2008) 5822.
[7] Y. Shigesato, T. Hayashi, T. Haranoh, Appl. Phys. Lett. 61 (1992) 73–75.
[8] T.J. Coutt, D.L. Young, X. Li, MRS Bull. 25 (2000) 58–65.
[9] A.V. Moholkar, S.M. Pawar, K.Y. Rajpure, V. Ganesan, C.H. Bhosale, J. Alloys Compd. 464 (2008) 387–392.
[10] L. Kong, J. Ma, F. Yang, C. Luan, Z. Zhu, J. Alloys Compd. 499 (2010) 75–79.
[11] M. Sasaki, K. Yasui, S. Kohiki, H. Deguchi, S. Matsushima, M. Oku, T. Shishido, J. Alloys Compd. 334 (2002) 205–210.
[12] T. Asikainen, M. Ritala, M. Leskela, Thin Solid Films 440 (2003) 152–154.
[13] H.K. Kim, C.C. Li, G. Nykolak, P.C. Becker, J. Appl. Phys. 76 (1994) 8209–8211.
[14] N. Ito, Y. Sato, P.K. Song, A. Kaijio, K. Inoue, Y. Shigesato, Thin Solid Films 496 (2006) 99–103.
[15] S. Kaleemulla, A. Sivasankar Reddy, S. Uthanna, P. Sreedhara Reddy, J. Alloys Compd. 479 (2009) 589–593.
[16] R. Sharma, R.S. Mane, S.K. Min, S.H. Han, J. Alloys Compd. 479 (2009) 840–843.
[17] L.P. Peng, L. Fang, X.F. Yang, Y.J. Li, Q.L. Huang, F. Wu, C.Y. Kong, J. Alloys Compd. 484 (2009) 575–579.
[18] S.Y. Sun, J.L. Haung, D.F. Lii, Thin Solid Films 469 (2004) 6–10.
[19] J.L. van der Pauw, Philips Res. Rep. 13 (1958) 1.
[20] Powder Diffraction File, No. 06-0413, JCPDS-International Center for Diffraction Data, Pennsylvania, 1972.
[21] C. Agashe, S. Mahamuni, Semicond. Sci. Technol. 10 (1995) 172–178.
[22] M.F.A.M. Van Hest, M.S. Dabney, J.D. Perkins, D.S. Ginley, Appl. Phys. Lett. 87 (2005) 32111–32113.
[23] H.J. Chun, Y.S. Choi, S.Y. Bae, H.C. Choi, J. Park, Appl. Phys. Lett. 85 (2004) 461–463.
[24] S. Parthiban, V. Gokulakrishnan, K. Ramamurthi, E. Elangovan, R. Martins, E. Fortunato, R. Ganesan, Sol. Energy Mater. Sol. Cells 93 (2009) 92–97.
[25] K.T.R. Reddy, H. Gopalaswamy, P.J. Reddy, R.W. Miles, J. Cryst. Growth 210 (2000) 516–520.
[26] L. Wang, L. Meng, V. Teixeira, S. Song, Z. Xu, X. Xu, Thin Solid Films 517 (2009) 3721–3725.
[27] Y.S. Song, J.K. Park, T.W. Kim, C.W. Chung, Thin Solid Films 467 (2004) 117–120.
[28] P. Prathap, N. Revathi, K.T.R. Reddy, R.W. Miles, Thin Solid Films 518 (2009) 1271–1274.
[29] R.J. Deokate, S.V. Salunkhe, G.L. Agawane, B.S. Pawar, S.M. Pawar, K.Y. Rajpure, A.V. Moholkar, J.H. Kim, J. Alloys Compd. 496 (2010) 357–363.
[30] D.J. Seo, S.H. Park, Phys. B: Condens. Matter 357 (2005) 420–427.
[31] B.G. Lewis, D.C. Paine, MRS Bull. 25 (2000) 22–27.
[32] A.J. Freeman, K.R. Poeppelmeier, T.O. Mason, R.P.H. Chang, T.J. Marks, MRS Bull. 25 (2000) 45–51.
[33] G. Frank, H. Kostlin, Appl. Phys. A: Solids Surf. 27 (1982) 197–200.
[34] C.C. Kuo, C.C. Liu, C.C. Lin, Y.Y. Liou, Y.F. Lan, J.L. He, Vacuum 82 (2008) 441–447.
[35] A.V. Moholkar, S.M. Pawar, K.Y. Rajpure, C.H. Bhosale, J. Alloys Compd. 455 (2008) 440.
[36] X. Li, W. Miao, Q. Zhang, L. Huang, Z. Zhang, Z. Hun, Semicond. Sci. Technol. 20 (2005) 823–828.